Yang, J., J. Su, J. C. Xia, C. Jin, X. Li and Q. Ge (2018). "The Impact of Spatial Form of Urban Architecture on the Urban Thermal Environment: A Case Study of the Zhongshan District, Dalian, China." IEEE Journal of Selected Topics in Applied Earth Observations and Remote Sensing 11(8): 2709-2716.

The Impact of Spatial Form of Urban Architecture on the Urban Thermal Environment: A Case Study of the Zhongshan District, Dalian, China

Jun Yang, Junru Su, Jianhong (Cecilia) Xia, Cui Jin, Xueming Li, Quansheng Ge

Abstract: **The correlation of spatial variation in land surface temperature (LST) with building height and density in Zhongshan District, Dalian, China is investigated over the period 2003–2013. We utilize remote sensing data and multi-source land use data, which we evaluate using a combination of a single-window algorithm and correlation analysis. The results show that: (1) During 2003–2013, the number of high surface temperature regions increased by 4,339 grid cells (out of a total of 53,601), with most of the high-temperature grid cells distributed along Jiefang Road and Zhongnan Road in the northern part of Zhongshan District. Ninety-eight percent of grid cells had temperature ranges of 293–309 K in July 2003, 296–310 K in August 2003, 295–308 K in July 2008, 296–311 K in August 2008, 305–314 K in July 2013, and 303–318 K in August 2013. (2) During 2003–2008, the number of low-rise buildings increased by 140%, and the number of multi-story buildings increased by 100%. During 2008–2013, the number of buildings in all height categories remained relatively unchanged, with the exception of an 11% decrease in the number of low-rise buildings. (3) Surface temperature showed weak correlation with building height (0.314 0.346, and 0.361 in 2003, 2008, and 2013, respectively) but moderate correlation with building density (0.511, 0.533, and 0.563, respectively).**

***Index Terms*—land surface temperature (LST); heat island effect; spatial and temporal evolution; building density; building height; correlation analysis; Zhongshan District, Dalian**

Manuscript received ; revised ; accepted . Date of publication ; date of current version . This work was supported in part by the Project of Natural Science Foundation of China under Grant 41771178 and Grant 41471140. (Corresponding author: Jun Yang.)

J. Yang is with the Liaoning Key Laboratory of Physical Geography and Geomatics, Liaoning Normal University, 116029, Dalian, China.(e-mail: yangjun@lnnu.edu.cn).

J. Su , C. Jin and X. Li are with the Liaoning Key Laboratory of Physical Geography and Geomatics, Liaoning Normal University, 116029, Dalian, China (e-mail: sujunru_ls@126.com; 174941792@qq.com; lixueming999@163.com).

J. Xia is with GIS at Department of Spatial Sciences, Curtin University, Australia (Email: c.xia@curtin.edu.au).

S. Ge is with Key Laboratory of Land Surface Pattern and Simulation, Institute of Geographic Sciences and Natural Resources Research, CAS, Beijing, China (Email: geqs@igsnrr.ac.cn).

I. INTRODUCTION

URBANIZATION and the rapid development of cities leads to fast growth of urban space [1, 2], which can cause a range of problems. Urban heat islands have a profound impact on the urban living environment, micro-climate, air quality, and urban public health, and also influence other climatic factors such as exacerbation of atmospheric pollution, change in the spatial distribution of precipitation, and change in vegetation phenology [3].

Many studies have measured surface temperature conditions using thermal infrared remote sensing through single-window algorithms, multi-channel algorithms, and other similar methods [4-6]. Single-channel algorithms [7-10] include atmospheric correction and single-window methods. In turn, the single-window method includes the single-window algorithm [11-15] and generalized single-channel algorithm methods [16], the split-window method [17-20], the multi-channel algorithm method [21-23], and both single- and multi-channel versions of the multi-angle method. Performing atmospheric correction using atmospheric simulations enables provision of accurate real-time atmospheric profile data. The window used in the single window algorithm is relatively wide, typically using the inversion of thermal infrared data to determine surface temperature. The split window method uses the inversion of the absorption characteristics of two adjacent bands of radiation in a specified atmospheric window, while the multi-channel synchronization algorithm relies on inversion using multi-spectral temperature and emissivity data.

The influence of different construction types on land surface temperature (LST) has been studied previously. Zhao et al. [24] studied the daytime and nighttime thermal effects of various types of building groups. Chun and Guldmann [25] and Chun and Guhathakurta [26] conducted regression analysis, considering building type and land use. Wu et al. [27] analyzed the impact of the urban thermal environment by comparing developed and unused land. Yang et al. [28] studied the urban heat island effect using three high-rise residential developments in Shanghai as an example and performed a regression analysis incorporating the building layout, building density, and vegetation cover. Wang and Ouyang [29] used the sky-view factor, building density, building height, and other factors as measures of land

surface usage. Du et al. [30] used building density in a regression analysis model to assess the influence of landscaping on the urban thermal environment. Stewart and Oke [31] and Ng et al. [32] studied the impact of the thermal environment on local climate zones by density on urban heat islands. Zhan et al. [35] explored the influence of ground coverage rate and construction volume density on land surface temperature. Through the study of various land coverage and construction patterns, Feng and Myint [36] explored LST in terms of the relationship between the central building structures in a neighborhood and the surrounding pattern of land coverage. Ge et al. [37] used visual interpretation to subdivide a study area into various building density zones, and used LST data obtained by remote sensing inversion to analyze the relationship between urban building density distribution and the urban heat island effect. On account of urban morphology and building height, Qiao et al. [38] used the Urban Ventilation Network Model (UVNM) to extract ventilation channels and verify their influence on urban surface temperature.

The spatial form of urban architecture is often considered when studying the urban thermal environment effect. The change in urban architectural form is an important feature of urban development. The vertical and horizontal expansion of urban architecture is used to characterize the vertical and horizontal development of the city. But this approach is still in need of improvement. Understanding the mechanisms behind the urban heat island effect and its variability has practical significance, with the potential to improve the urban living environment and conduct more careful planning of urban development. Such understanding also has theoretical significance for the study of global and regional climate change. In this study, we combine Landsat 8 and Landsat 5 images with other data sources. Specifically, we use Landsat 8 thermal infrared band 10 and Landsat 5 thermal infrared band 6 for estimation of LST and combine these data with records of building height and building density. Using a bivariate correlation model, we analyze the influence of urbanization and building height/density on surface temperature. We analyze the thermal environment effect resulting from the evolution of urban building types associated with rapid urbanization by studying the relationship between the pixel patterns of structures in an area and urban surface temperatures, thus providing a theoretical basis for study of the thermal environment effect, with the aim of addressing some of the practical problems associated with urban development.

II. Study area and data sources

A. Study area

Zhongshan is a district governed by Dalian City in Liaoning Province, China and is located in the southeast part of the Dalian urban area (121°37′15″E–121°43′3″E, 38°51′37″N–38°56′17″N). The eastern, considering building density. Weng et al. [33] considered residential land by studying building types and suggested that residential land has a lower surface temperature than commercial or industrial land. Kammuang-Lue et al. [34] studied the effects of population, buildings, and traffic southern, and northern boundaries of Zhongshan District are adjacent to the ocean, while the western side borders Xigang District. Our study area matches the current administrative boundaries of Zhongshan District (see Fig. 1).

B. Data pre-processing

Original data sources consisted of Landsat 8 OLI and TIRS data and Landsat 5 TM images (see Table Ⅰ), together with reference data consisting of weather statistics for the study area. Using three remote sensing images, acquired within a month, minimizes the error caused by climate. Remote sensing data are calibrated by radiometric calibration and atmospheric correction to eliminate the errors caused by the sensor itself and those caused by atmospheric scattering, absorption, and reflection. Relative humidity in the research area was estimated by comparing the OLI, TIRS, and TM images with the corresponding MODIS atmospheric temperature and humidity profile (MOD07) products for the same period. MOD07 estimates relative humidity using an empirical relationship between surface water vapor pressure and atmospheric precipitation [39-41].

III. Methodology

A. Technical roadmap

A grid was applied to the study area, dividing it into 53,601 grid squares. The study of the spatiotemporal evolution of urban construction and the urban thermal environment effect is divided into three main components: (1) the urban thermal environment effect, measured using surface temperature obtained through the single-window algorithm, and surface temperature distribution conditions and their evolutionary characteristics; (2) the spatiotemporal evolution of urban building heights and densities; (3) bivariate correlation analysis of LST, building height, and building density. Fig. 2 shows this study process in detail.

B. Building height and density

Building height refers to the height difference between the roof and the outdoor surface. Building density (%) refers to the ratio between the total base area of buildings and the total area of a specific region. In this paper, building density refers to the ratio of base area to grid area (30 m × 30 m). Building height and density are important for evaluating the spatial distribution of buildings in an area [31, 42]. We classify building height and density in Tables Ⅱ and Ⅲ, respectively.

C. Single-window algorithm

This study employs the single-window algorithm proposed by proposed Qin et al. [15], Wang et al. [13], and Tu et al. [12]. This method considers parameters including land surface emissivity, atmospheric transmittance, brightness temperature, and atmospheric mean temperature, and then calculates surface temperature using equations 1 to 3:

$$T_s=\{a(1-C-D)+[b(1-C-D)+C+D]T-DT_a\}/C \quad (1)$$

$$C=\tau\varepsilon \quad (2)$$

$$D=(1-\tau)[(1-\varepsilon)\tau] \quad (3)$$

where a and b are coefficients obtained from the relationship between thermal radiation intensity and brightness temperature，a = -70.1775, b = 0.4581; ε is ground emissivity; τ is total atmospheric transmittance; T is at-sensor brightness temperature; and T_a is mean atmospheric temperature (K).

1) Brightness temperature

TIRS band 10 and TM band 6 data are thermal infrared bands with corresponding pixel brightness temperatures as follows:

$$T=K_2/\ln(K_1/L_\lambda+1) \quad (4)$$

Where L_λ is radiation intensity received by the sensor; K_1 and K_2 are pre-launch preset constants found in the Landsat 8 and Landsat 5 header files (Table Ⅳ):

TABLE Ⅳ
THERMAL CONSTANT VALUES

Thermal constant	Landsat 8, band 10	Landsat 5, band 6
K_1	774.89	607.76
K_2	1321.08	1260.56

2) Calculating mean atmospheric temperature

Mean atmospheric temperature (T_a) generally depends on the profile of atmospheric air temperature distribution and atmospheric conditions. Qin et al. [11] and Wang et al. [13] demonstrated that mean atmospheric temperature (T_a) has a linear relationship with near-surface temperature (T_0). We obtain T_0 is from the same period of MOD07 data. Given that the study area is located in the mid-latitudes and that the images were acquired during July and August, mean mid-latitude summer atmospheric conditions were therefore used (Table 4).

$$T_a=16.0110+0.9262T_0 \quad (5)$$

3) Calculating atmospheric transmittance rate

Atmospheric transmittance is calculated using information about water vapor, wavelength, ozone, and aerosols. Of these, water vapor is the most important factor for atmospheric transmittance variation within the spectral temperature range [43] (see Table Ⅴ):

$$\omega_i=0.0981*\left\{10*0.6108*\exp\left[\frac{17.27*(T_0-273.15)}{273.3+(T_0-273.15)}\right]RH\right\}+0.1697 \quad (6)$$

Where τ represents transmittance rate; ω_i represents atmospheric vapor content; (T_0) represents near-surface temperature; and RH represents relative humidity. T_0 and RH are obtained from the same period of MOD07 data.

4) Calculating ground emissivity

The pixel-scale images of the Earth's surface are not homogenous; instead, over the study area, we assign pixels as representing either a water body, urban land, or a natural surface (i.e., unused land). The boundaries between water bodies and dry land are relatively sharp, and the pixels are fairly uniform and easy to extract, with an emissivity of 0.995. The emissivities of urban land and natural surfaces are calculated using equations 7 and 8, respectively; vegetation indices are calculated using equations 9 and 10 [44]. The relationship between emissivity and vegetation indices is presented in Table Ⅵ.

$$\varepsilon_{urban}=0.9608+0.0860F_v-0.0671F_v^2 \quad (7)$$

$$\varepsilon_{surface}=0.9644+0.0615F_v-0.0461F_v^2 \quad (8)$$

$$F_v=(NDVI-NDVI_s)/(NDVI_v-NDVI_s) \quad (9)$$

$$NDVI=(NIR-RED)/(NIR+RED) \quad (10)$$

where, ($\varepsilon_{surface}$) and (ε_{urban}) are the emissivity of natural surface and urban land surface pixels, respectively; (F_v) is vegetation coverage; NDVI is normalized difference vegetation index; ($NDVI_v$) is the vegetation index of vegetation; ($NDVI_s$) is the vegetation index of soil.

D. Bivariate correlation analysis

Bivariate correlation analysis is used primarily with two or more variables. Based on the data type, different correlation coefficients can be used to measure the linear correlations between variables. The most common forms are the Pearson simple, Spearman's rank, and Kendall's tau-b concordance correlation coefficients. Here, we employ the Pearson simple correlation coefficient

$$r=\frac{\sum(x-\bar{x})(y-\bar{y})}{\sqrt{\sum(x-\bar{x})^2\sum(y-\bar{y})^2}} \quad (11)$$

The statistical test corresponding to the Pearson simple correlation coefficient is the t-statistic. SPSS software automatically provides the corresponding t-statistic probability, based on the t-statistic and the degrees of freedom in accordance with the t distribution table.

IV. Results

A. Building height and density distribution

The Code for Design of Civil Buildings divides structures into five categories according to height: low-rise, multi-story, middle-high, high-rise, and super high-rise [42].

We now consider the evolution of the spatial distribution of buildings low-rise, multi-story, and middle-high buildings were the most common structures in Zhongshan District, and they were mainly concentrated in the northwestern and central parts of

the district (Jiefang Road and Zhongnan Road). Only small proportions of high-rise and super high-rise buildings were present, and these were located mainly in the Qingniwa-Tianjin Street commercial district (which includes Qingni and People's Road sub-districts, and the northeastern area of Kunming sub-district) (Figs. 3 and 4).

In Fig. 5a, we illustrate how building numbers increased during 2003–2008, with a particularly strong rise in numbers of low-rise (140% increase) and multi-story (100% increase) buildings. During 2008–2013, the number of buildings in all height categories remained relatively unchanged, with the exception of the number of low-rise buildings, which decreased by 11%.

We now consider building density. The high- and relatively high-density plots were distributed mainly in the commercial district of Qingniwa-Tianjin Street (including the Qingni and People's Road sub-districts, and the northeastern area of Kunming sub-district). Most of the low-, relatively low-, and medium-density plots were distributed along Jiefang Road and Zhongnan Road. During 2003–2013, the high- and relatively high-density plots in Guilin and Navy Square sub-districts turned into medium- and relatively low-density plots; meanwhile, building density showed a clear increase in the middle of the study area (Figs. 5b and 6).

B. Surface temperature distribution

The experimental results show that the error between the calculated LST and the measured LST is less than 5%, which can reflect the spatial distribution of the LST in the study area.

We now consider the evolution of the spatial distribution of surface temperature. The temperature in the north and along Jiefang Road and Zhongnan Road is relatively high, and the temperature in the east and south is relatively low. In July 2003, 98% of grid cells had a temperature within the range 293–309 K. In August 2003, 98% of grid cells had a temperature within the range 296–310 K. In July 2008, 98% of grid cells had a temperature within the range 295–308 K. In August 2008, 98% of grid cells had a temperature within the range 296–311 K. In July 2013, 98% of grid cells had a temperature within the range 205–314 K. In August 2013, 98% of grid cells had a temperature within the range 303–318 K (Figs. 7 and 8).

During 2003–2008, the temperature in the northwest portion of the study area and the Zhongnan Road and Jiefang Road increased significantly. During 2008–2013, the temperature increased throughout the study area. Due to land reclamation in the northwest portion of the study area, the temperature increased sharply. The temperature increased significantly after an area of land in the northeastern part of the district was reclaimed from the ocean. In addition, many low- and middle-high buildings in the northwestern and western parts had been converted to high-rise buildings (Figs. 7 and 8).

C. Correlation of surface temperature with building height and density

The average annual temperature for two months was calculated, and the correlation between the surface temperature and the building height and the building density was then analyzed. Table Ⅶ shows the results of correlation analysis for surface temperature, building height, and building density for 2003, 2008, and 2013. Our results show that surface temperature correlates only weakly with building height (0.314, 0.346, and 0.361 in 2003, 2008, and 2013, respectively), but moderately with building density (0.511, 0.533, and 0.563). There is a low positive correlation between LST and building height, which indicates that high-rise buildings have a small effect on LST. The surface temperature and building density have a moderate correlation, which indicates that the high-density building area has a relatively large impact on the LST.

V. Discussion and Conclusions

A. Discussion

The Dalian Municipal Planning Bureau issued the relevant provisions of the planning and design of Dalian city notice on August 24, 2005, which is used for the construction, management and protection of the city. The height of the building and the density of the building are clearly stipulated in the provisions. There is an increase in the height of urban buildings, the middle and relatively high building density and the surface temperature. It is necessary to strictly implement the relevant provisions and pay attention to the planning.

In this study, the single window algorithm is used to retrieve the LST. Because it is difficult to eliminate the influence of the atmosphere using this algorithm, Landsat imagery with a cloud coverage less than 5% was selected. The building density in this study refers to the ratio of the base area to the grid area (30 m× 30 m). In the next study, the grid scale can be adjusted in order to get a better scale. The selected correlation analysis method has effectively analyzed the correlation between LST and building height and density, but this method cannot well express their spatial correlation.

We focused on characterizing the potential relationships between building height/density and the heat island effect. However, many other factors are also involved, e.g., roads and vegetation. These factors should be taken into account in a future comprehensive analysis. Our study is also limited by errors in the remote sensing band algorithm. The mechanisms behind the heat island effect therefore require further study and analysis using high-precision, long-term, and multiple-period data sets.

B. Conclusions

Our study investigates the effects of the rapid urbanization of Zhongshan District, Dalian, on the thermal environment. We utilized surface temperatures and bivariate correlations to analyze spatial and temporal changes associated with urban buildings. We determined surface temperatures using the single-window algorithm, and employed bivariate correlation analysis to explore possible associations of building height and density with surface temperature, and obtained the following results:

1) The number of buildings increased during 2003–2008, especially in the low-rise and multi-story building categories. The number of low-rise and multi-story buildings increased by 140% and 100%, respectively. In this period, urban buildings are growing in two directions, both horizontal and vertical, and the urban space is growing rapidly. During 2008–2013, building numbers in all height categories remained relatively unchanged, except for a decrease of 11% in the number of low-rise buildings. In this period of time, urban buildings have mainly vertical growth.
2) Surface temperature data show that the number of high-temperature grid cells increased significantly, by 4,339 (out of a total of 53,601), between 2003 and 2013. Most of the high-temperature grid cells were distributed along Jiefang Road and Zhongnan Road in the northern part of Zhongshan District. Our results show that 98% of grid cells had temperatures of 293–309 K in July 2003, 296–310 K in August 2003, 295–308 K in July 2008, 296–311 K in August 2008, and 305–314 K in July 2013, and 303–318 K in August 2013. The distribution of surface temperature is basically consistent with the distribution of buildings and the distribution of building density. Urban low building density area has more green and empty space, the air ventilation efficiency is high, the temperature is relatively low. In contrast, the temperature is relatively high in the urban high building density area.
3) In 2003, 2008, and 2013, surface temperature showed low correlation with building height (correlation coefficients of 0.314, 0.346, and 0.361, respectively), but moderate correlation with building (0.511, 0.533, and 0.563, respectively). When the number of urban buildings increases, the ventilation efficiency in the area is reduced and the temperature is relatively high. Conversely, the urban low building density area has more greening, which is convenient for air circulation and results in relatively low temperature.

REFERENCES:

[1] Q. He, Y. Liu, C. Zeng, C. Yin and R. Tan, "Simultaneously simulate vertical and horizontal expansions of a future urban landscape: a case study in Wuhan, Central China," *INT J GEOGR INF SCI*, 1, pp.1-22,2017.

[2] Y. Liu, Q. He, R. Tan, Y. Liu and C. Yin, "Modeling different urban growth patterns based on the evolution of urban form: A case study from Huangpi, Central China," *Applied Geography*, vol.66,no.pp.109-118,2016.

Y. Chen, J. Zhou, E. Gong, W. Ma and W. Zhan, *Urban space thermal environment remote sensing*, Science Press (2014).

[4] H. Feng, H. Liu and L. Wu, "Monitoring the Relationship Between the Land Surface Temperature Change and Urban Growth in Beijing, China," *IEEE Journal of Selected Topics in Applied Earth Observations & Remote Sensing*, vol.7,no.10, pp.4010-4019,2014.

[5] B. H. Tang, C. Zhan, Z. L. Li, H. Wu and R. Tang, "Estimation of Land Surface Temperature From MODIS Data for the Atmosphere With Air Temperature Inversion Profile," *IEEE Journal of Selected Topics in Applied Earth Observations & Remote Sensing*, vol.PP,no.99, pp.1-8,2017.

[6] J. Zhou, X. Zhang, W. Zhan, F. M. Göttsche, S. Liu, F. S. Olesen, W. Hu and F. Dai, "A Thermal Sampling Depth Correction Method for Land Surface Temperature Estimation From Satellite Passive Microwave Observation Over Barren Land," *IEEE Transactions on Geoscience & Remote Sensing*, vol.PP,no.99, pp.1-14,2017.

[7] S. Bonafoni, "Downscaling of Landsat and MODIS Land Surface Temperature Over the Heterogeneous Urban Area of Milan," *IEEE Journal of Selected Topics in Applied Earth Observations & Remote Sensing*, vol.9,no.5, pp.2019-2027,2016.

[8] Y. Chen and S. Yu, "Impacts of urban landscape patterns on urban thermal variations in Guangzhou, China," *International Journal of Applied Earth Observation & Geoinformation*, vol.54,no.pp.65-71,2017.

[9] C. Hutengs and M. Vohland, "Downscaling land surface temperatures at regional scales with random forest regression," *REMOTE SENS ENVIRON*, vol.178,no.pp.127-141,2016.

[10] J. C. Jimenezmunoz, J. Cristobal, J. A. Sobrino, G. Soria, M. Ninyerola, X. Pons and X. Pons, "Revision of the single-channel algorithm for land surface temperature retrieval from Landsat thermal-infrared data.," *IEEE Transactions on Geoscience & Remote Sensing*, vol.47,no.1, pp.339-349,2009.

[11] Z. Qin, A. Karnieli and P. Berliner, "A mono-window algorithm for retrieving land surface temperature from Landsat TM data and its application to the Israel-Egypt border region," *INT J REMOTE SENS*, vol.22,no.18, pp.3719-3746,2001.

[12] L. Tu, Z. Qin, W. Li, J. Geng, L. Yang, S. Zhao, W. Zhan and F. Wang, "Surface urban heat island effect and its relationship with urban expansion in Nanjing, China," *J APPL REMOTE SENS*, vol.10,no.2, pp.26037,2016.

[13] F. Wang, Z. Qin, C. Song, L. Tu, A. Karnieli and S. Zhao, "An Improved Mono-Window Algorithm for Land Surface Temperature Retrieval from Landsat 8 Thermal Infrared Sensor Data," *REMOTE SENS-BASEL*, vol.7,no.4, pp.4268-4289,2015.

[14] X. Zhang, Y. Hu, G. Jia, M. Hou, Y. Fan, Z. Sun and Y. Zhu, "Land surface temperature shaped by urban fractions in megacity region," *Theoretical & Applied Climatology*, pp.1-11,2015.

[15] Q. Zhi-Hao, M. Zhang and A. Karnieli, "Mono-window algorithm for retrieving land surface temperature from Landsat TM6 data," *ACTA GEOGRAPHICA SINICA-CHINESE EDITION-*, vol.56,no.4, pp.466-474,2001.

[16] J. C. Jiménez-Muñoz and J. A. Sobrino, "A generalized single-channel method for retrieving land surface temperature from remote sensing data," *Journal of Geophysical Research Atmospheres*, vol.108,no.D22, pp.2015-2023,2003.

[17] Y. Chen, S. B. Duan, H. Ren, J. Labed and Z. L. Li, "Algorithm Development for Land Surface Temperature Retrieval: Application to Chinese Gaofen-5 Data," *REMOTE SENS-BASEL*, 2, pp.161,2017.

[18] C. Gao, S. Qiu, E. Y. Zhao, C. Li, L. L. Tang, L. L. Ma, X. Jiang, Y. Qian, Y. Zhao and N. Wang, "Land Surface Temperature Retrieval From FY-3C/VIRR Data and Its Cross-Validation With Terra/MODIS," *IEEE Journal of Selected Topics in Applied Earth Observations & Remote Sensing*,

vol.PP,no.99, pp.1-10,
[19] S. A. Nowicki, "Thermophysical Characterization of the Southwestern U.S. From 5 Years of MODIS Land Surface Temperature Observations," *IEEE Journal of Selected Topics in Applied Earth Observations & Remote Sensing*, vol.7,no.8, pp.3416-3420,2014.
[20] X. Ye, H. Ren, R. Liu, Q. Qin, Y. Liu and J. Dong, "Land Surface Temperature Estimate From Chinese Gaofen-5 Satellite Data Using Split-Window Algorithm," *IEEE Transactions on Geoscience & Remote Sensing*, vol.PP,no.99, pp.1-12,2017.
[21] V. García-Santos, C. Coll, E. Valor, R. Niclòs and V. Caselles, "Analyzing the anisotropy of thermal infrared emissivity over arid regions using a new MODIS land surface temperature and emissivity product (MOD21)," *REMOTE SENS ENVIRON*, vol.169,no.pp.212-221,2015.
[22] J. A. Sobrino, J. C. Jiménez-Muñoz, P. J. Zarco-Tejada, G. Sepulcre-Cantó and E. D. Miguel, "Land surface temperature derived from airborne hyperspectral scanner thermal infrared data," *REMOTE SENS ENVIRON*, vol.102,no.1–2, pp.99-115,2006.
[23] Z. Wan and Z. L. Li, "A physics-based algorithm for retrieving land-surface emissivity and temperature from EOS/MODIS data," *IEEE Transactions on Geoscience & Remote Sensing*, vol.35,no.4, pp.980-996,1997.
[24] G. Zhao, J. Dong, J. Liu, J. Zhai, Y. Cui, T. He and X. Xiao, "Different Patterns in Daytime and Nighttime Thermal Effects of Urbanization in Beijing-Tianjin-Hebei Urban Agglomeration," *REMOTE SENS-BASEL*, pp.121,2017.
[25] B. Chun and J. M. Guldmann, "Spatial statistical analysis and simulation of the urban heat island in high-density central cities," *Landscape & Urban Planning*, vol.125,no.3, pp.76-88,2014.
[26] B. Chun and S. Guhathakurta, "The Impacts of Three-Dimensional Surface Characteristics on Urban Heat Islands over the Diurnal Cycle," *The professional Geographer*, vol.69,no.2, pp.191-202,2017.
[27] H. Wu, L. P. Ye, W. Z. Shi and K. C. Clarke, "Assessing the effects of land use spatial structure on urban heat islands using HJ-1B remote sensing imagery in Wuhan, China," *International Journal of Applied Earth Observation & Geoinformation*, vol.32,no.1, pp.67-78,2014.
[28] F. Yang, S. S. Y. Lau and F. Qian, "Summertime heat island intensities in three high-rise housing quarters in inner-city Shanghai China: Building layout, density and greenery," *Building & Environment*, vol.45,no.1, pp.115-134,2010.
[29] J. Wang and W. Ouyang, "Attenuating the surface Urban Heat Island within the Local Thermal Zones through land surface modification.," *J ENVIRON MANAGE*, vol.187,no.pp.239,2017.
[30] S. Du, Z. Xiong, Y. C. Wang and L. Guo, "Quantifying the multilevel effects of landscape composition and configuration on land surface temperature," *REMOTE SENS ENVIRON*, vol.178,no.pp.84-92,2016.
[31] I. D. Stewart and T. R. Oke, "Local Climate Zones for Urban Temperature Studies," *B AM METEOROL SOC*, vol.93,no.12, pp.1879-1900,2012.
[32] Y. X. Y. Ng, L. H. C. Chua and K. N. Irvine, "A study of urban heat island using "local climate zones" - the case of Singapore.," *British Journal of Environment & Climate Change*, vol.5,no.2, pp.116-133,2015.
[33] Q. Weng, P. Fu and F. Gao, "Generating daily land surface temperature at Landsat resolution by fusing Landsat and MODIS data," *REMOTE SENS ENVIRON*, vol.145,no.8, pp.55-67,2014.
[34] N. Kammuang-Lue, P. Sakulchangsatjatai, P. Sangnum and P. Terdtoon, "Influences of population, building, and traffic densities on urban heat island intensity in Chiang Mai Sity, Thailand," *THERM SCI*, 00, pp.85,2015.
[35] Q. Zhan, F. Meng and Y. Xiao, "Exploring the relationships between land surface temperature, ground coverage ratio and building volume density in an urbanized envronment," *International Archives of the Photogrammetry Remote Sensing & S*, vol.XL-7/W3,no.7, pp.255-260,2015.
[36] X. Feng and S. W. Myint, "Exploring the effect of neighboring land cover pattern on land surface temperature of central building objects," *Building & Environment*, vol.95,no.pp.346-354,2016.
[37] Y. Ge, X. Xu, J. Li, H. Cai and X. Zhang, "Study on the Influence of Urban Building Density on the Heat Island Effect in Beijing," *Journal of Geo-information*, vol.18,no.12, pp.1698-1706,2016.
[38] Z. Qiao, X. Xu, F. Wu, W. Luo, F. Wang, L. Liu and Z. Sun, "Urban ventilation network model: a case study of the core zone of capital function in Beijing metropolitan area," *J CLEAN PROD*, 2017.
[39] H. Adab, K. D. Kanniah, K. Solaimani and K. P. Tan, "Estimating atmospheric humidity using MODIS cloud-free data in a temperate humid region," *Geoscience & Remote Sensing Society*, pp.1827-1830,2013.
[40] G. X. Peng, L. I. Jing, Y. H. Chen and N. A. Patah, "A METHOD OF ESTIMATING RELATIVE HUMIDITY FROM MODIS ATMOSPHERIC PROFILE PRODUCTS," *J TROP METEOROL*, vol.23,no.6, pp.611-616,2007.
[41] J. Yang, J. Sun, Q. Ge and X. Li, "Assessing the Impacts of Urbanization-Associated Green Space on Urban Land Surface Temperature: A Case Study of Dalian, China," *URBAN FOR URBAN GREE*, vol.22,no.pp.1-10,2017.
[42] The Ministry of Construction of the People's Republic of China, "Code for Design of Civil Buildings," in *GB 50352-2005*, China Architecture & Building Press (2005).
[43] B. F. Bektaş, "Determining the impact of urban components on land surface temperature of Istanbul by using remote sensing indices," *Environmental Monitoring & Assessment*, vol.186,no.2, pp.859-872,2014.
[44] J. A. Sobrino, N. Raissouni and Z. L. Li, "A Comparative Study of Land Surface Emissivity Retrieval from NOAA Data," *REMOTE SENS ENVIRON*, vol.75,no.2, pp.256-266,2001.

Jun Yang, PhD is a Professor in the effect of human settlement and GIS at Liaoning Normal University.

He has been committed to urban space growth, urban thermal environment, cellular automata land use change, and urban human settlements, as well as other aspects of research.

Junru Su is currently working toward her Master's degree in cartography and geographic information systems at Liaoning Normal University, Dalian, China.

Her current research interests include urban thermal infrared remote sensing, urban space growth, and urban ventilation.

Jianhong (Cecilia) Xia has over 10 years' experience as a GIS educator, spatial analyst, and modeler.

She has also worked as a transport geographer and transit planner with a range of research experience in relation to tourism, public transport development, driving, spatial navigation and way finding, and human mobility.

Cui Jin, PhD is currently working at Liaoning normal University.

She works in the field of global climate change remote sensing, vegetation carbon cycling remote sensing, agricultural remote sensing, and land use and land cover change research.

Xuming Li, PhD, Professor is mainly engaged in urban human settlement environments and ecology, physical geography, and other teaching and research work.

Quansheng Ge, PhD, Professor is a Research Fellow whose main research area is global change. He is the current director of the Institute of Geographic Sciences and Natural Resources Research.

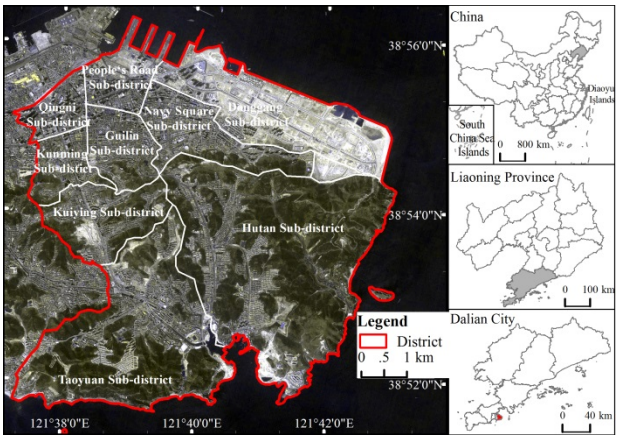

Fig 1. Map of the study area.

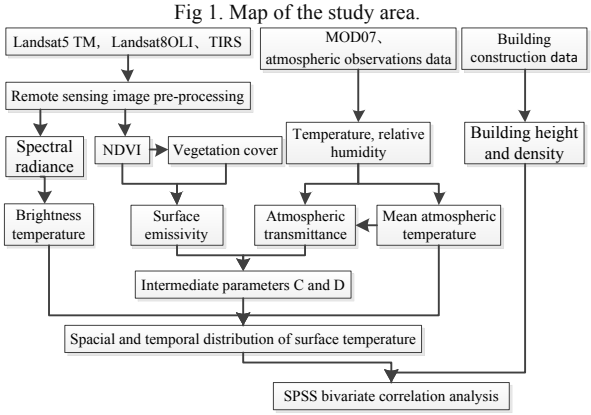

Fig. 2 Technology road map.

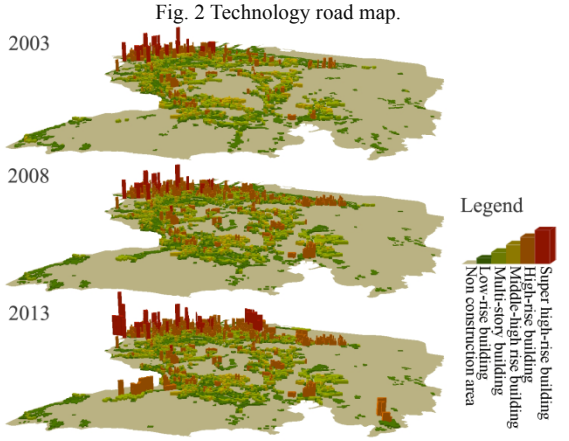

Fig. 3 Three-dimensional map of building distribution (actual height*3).

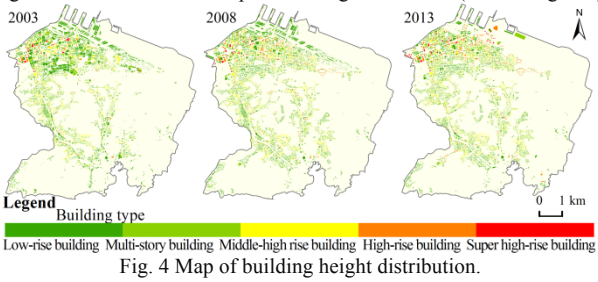

Fig. 4 Map of building height distribution.

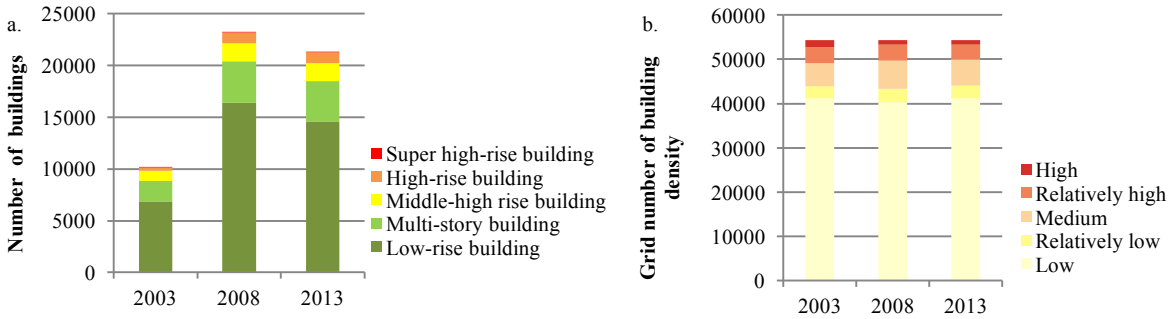

Fig. 5 Histograms showing: a. Numbers of buildings according to height; b. Numbers of spatial grid cells according to building density.

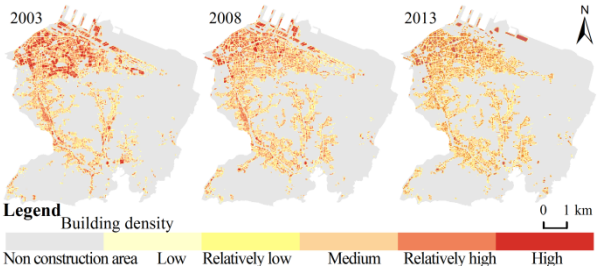

Fig. 6 Map of building density distribution.

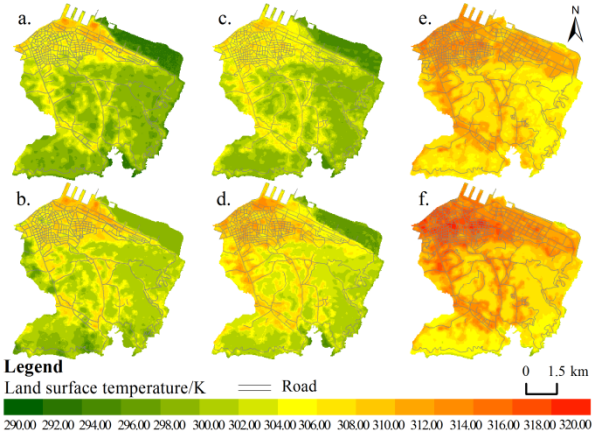

Fig. 7 Map of land surface temperature distribution showing: a. LST of July 2003; b. LST of August 2003; c. LST of July 2008; d. LST of August 2008; e. LST of July 2013; and f. LST of August 2013.

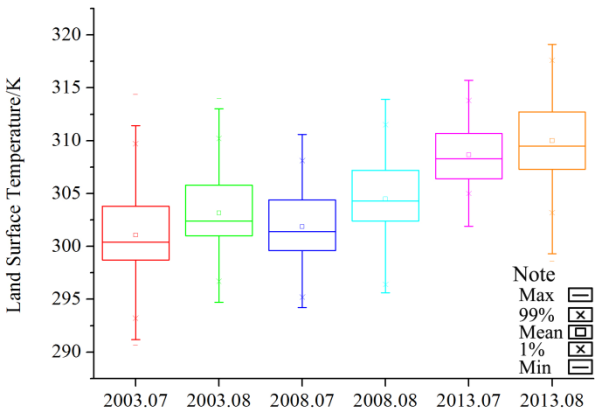

Fig. 8 Box plots of surface temperature distributions.

TABLE Ⅰ
DATA SOURCES AND DESCRIPTIONS

Date	Detector	Resolution	Data Sources
2013-07-03/2013-08-11	Landsat 8 OLI/TIRS	30 m	Geospatial Data Cloud
	MOD07 atmospheric broadband product	5 km	Downloaded from NASA
2013-08-05	SPOT5	10 m	National Bureau of Oceanography
2008-07-12/2008-08-06	Landsat 5 TM	30 m	Geospatial Data Cloud
	MOD07 atmospheric broadband product	5 km	Downloaded from NASA
2007-04-13	SPOT5	10 m	National Bureau of Oceanography
2003-07-15/2003-08-16	Landsat 5 TM	30 m	Geospatial Data Cloud
	MOD07 atmospheric broadband product	5 km	Downloaded from NASA
2003-06-16	SPOT5	10 m	National Bureau of Oceanography
2013	country, province, city, county (district), village (town, street) data	-	Dalian Planning Bureau
2003/2008/2013	building structure outline, height, the number of floors (stories)	-	Dalian Land Resource and Housing Bureau, SPOT image interpretation
2003/2008/2013	Roads	-	Dalian Land Resource and Housing Bureau

TABLE Ⅱ
CLASSIFICATION OF BUILDING TYPES [31, 42]

Building type	Classification standard
Low-rise building	1–3 floors (3–10 m)
Multi-story building	4–6 floors (10–18 m)
Middle-high rise building	7–9 floors (18–24 m)
High-rise building	10 or more floors (24–100 m)
Super high-rise building	Building height exceeds 100 m

TABLE Ⅲ
CLASSIFICATION OF BUILDING DENSITY [31, 42]

Building density	Classification standard
Low	0–10%
Relatively low	10–20%
Medium	20–40%
Relatively high	40–70%
High	70–100%

TABLE Ⅳ
THERMAL CONSTANT VALUES

Thermal constant	Landsat 8, band 10	Landsat 5, band 6
K_1	774.89	607.76
K_2	1321.08	1260.56

TABLE Ⅴ
DERIVATION OF ATMOSPHERIC TRANSMITTANCE

Atmospheres	Atmosphere vapor content (g*cm)	Transmittance estimation equation
Mid-Latitude average summer atmosphere	0.2–1.6	$\tau=0.9184-0.0825\omega_i$
	1.6–4.4	$\tau=1.0163-0.1330\omega_i$
	4.4-5.4	$\tau=0.7029-0.0620\omega_i$

TABLE Ⅵ
EQUATIONS AND CONDITIONS FOR ESTIMATING GROUND EMISSIVITY WITH NDVI THRESHOLD METHOD

NDVI value	Ground emissivity equation
NDVI<=0	Water body ε=0.995
0<NDVI<0.7	Urban land ε_{urban}
NDVI>=0.7	Natural surface $\varepsilon_{surface}$

TABLE Ⅶ
CORRELATIONS BETWEEN SURFACE TEMPERATURE AND BUILDING HEIGHT / DENSITY, 2003–2013

	2003		2008		2013	
	Building height	Building density	Building height	Building density	Building height	Building density
2003 land surface temperature	.314**	.511**	-	-		
2008 land surface temperature	-	-	.346**	.533**	-	-
2013 land surface temperature	-	-	-	-	.361**	.563**

**. Significant correlation at the 0.01 level (bilateral).